Epitaxial Versus Polycrystalline Shape Memory Cu-Al-Ni Thin Films

Doga Bilican [1], Samer Kurdi [2] , Yi Zhu [2], Pau Solsona [1], Eva Pellicer [1] , Zoe H. Barber [2], Alan Lindsay Greer [2], Jordi Sort [1,3] and Jordina Fornell [1,*]

[1] Departament de Física, Facultat de Ciències, Universitat Autònoma de Barcelona, E-08193 Bellaterra (Cerdanyola del Vallès), Spain; bilican.doga@gmail.com (D.B.); pau.solsona@uab.cat (P.S.); Eva.pellicer@uab.cat (E.P.); jordi.sort@uab.cat (J.S.)

[2] Department of Materials Science and Metallurgy, University of Cambridge, Cambridge CB3 0FS, UK; sk862@cam.ac.uk (S.K.); yz475@cam.ac.uk (Y.Z.); zb10@cam.ac.uk (Z.H.B.); alg13@cam.ac.uk (A.L.G.)

[3] Institució Catalana de Recerca i Estudis Avançats (ICREA), Pg. Lluís Companys 23, E-08010 Barcelona, Spain

* Correspondence: jordina.fornell@uab.cat; Tel.: +34-9358-114-01

check for updates

Abstract: In this work, two different approaches were followed to obtain Cu-Al-Ni thin films with shape memory potential. On the one hand, Cu-Ni/Al multilayers were grown by magnetron sputtering at room temperature. To promote diffusion and martensitic/austenitic phase transformation, the multilayers were subjected to subsequent heat treatment at 800 °C and quenched in iced water. On the other hand, Cu, Al, and Ni were co-sputtered onto heated MgO (001) substrates held at 700 °C. Energy-dispersive X-ray spectroscopy, X-ray diffraction, and transmission electron microscopy analyses were carried out to study the resulting microstructures. In the former method, with the aim of tuning the thin film's composition, and, consequently, the martensitic transformation temperature, the sputtering time and applied power were adjusted. Accordingly, martensitic Cu-14Al-4Ni (wt.%) and Cu-13Al-5Ni (wt.%) thin films and austenitic Cu-12Al-7Ni (wt.%) thin films were obtained. In the latter, in situ heating during film growth led to austenitic Cu-12Al-7Ni (wt.%) thin films with a (200) textured growth as a result of the epitaxial relationship MgO(001)[100]/Cu-Al-Ni(001)[110]. Resistance versus temperature measurements were carried out to investigate the shape memory behavior of the austenitic Cu-12Al-7Ni (wt.%) thin films produced from the two approaches. While no signs of martensitic transformation were detected in the quenched multilayered thin films, a trend that might be indicative of thermal hysteresis was encountered for the epitaxially grown thin films. In the present work, the differences in the crystallographic structure and the shape memory behavior of the Cu-Al-Ni thin films obtained by the two different preparation approaches are discussed.

Keywords: Cu-Al-Ni; shape memory alloys; thin film; sputtering; size effects

1. Introduction

Shape memory alloys (SMA) exhibit displacive and reversible deformation behavior due to sensing thermodynamic and mechanical changes in their environment [1–7]. This plays a role in the development of components that can be cycled between two macroscopic shapes depending on temperature change. The fact that SMAs exhibit temperature-induced strain recovery makes them a type of advanced engineering material. Typical application fields for these materials are encountered in sensing–actuating systems in automotive, aerospace, robotics, and biomedical technologies [8]. Of the most functional shape memory alloys, Ni-Ti [9–11] Cu-Zn-Al [12], and Cu-Al-Ni [13,14] are some of the most widely used. Even though the Ni-Ti SMA system is widely studied and commercialized on account of its high percentage of shape recovery, Cu-based SMAs have become long-term proposed

substitutions for the Ni-Ti system due to the fact that they have lower production costs in addition to having desirable properties such as a large superelastic effect, wide transformation temperature ranges, small hysteresis, and a high damping coefficient. Despite the fact that Fe-based SMAs, such as Fe-Mn and Fe-Mn-Si, also appear as substitute candidates for Ni-Ti due to their good workability and cost efficiency advantages, Fe-based SMAs undergo a large transformation hysteresis which limits their area for shape memory applications compared to Cu-based SMAs [15].

Regardless of the alloy composition, because of possessing large amounts of thermal capacitance, the application of shape memory behavior in bulk alloys is challenging. However, due to high actuation outputs per unit volume, the response time can be reduced substantially and the speed of operation may be increased sufficiently in shape memory thin films. As a consequence, these materials can be utilized in micro/nanorobotic platforms [16].

Rather than conventional elastic or plastic dislocation glide, the behavior of shape memory depends on displacive, diffusionless phase transformation, which takes place between a high temperature phase (austenite) and a low temperature one (martensite). As a non-equilibrium phase, the most commonly applied way to induce martensite in materials is to subject them to quenching after holding them at high temperature in order for the atoms to become locked into position before they reach their equilibrium states, with the lowest free energy [17]. Post-quenching is also convenient for introducing the shape memory effect in films grown at room temperature. Investigations on the synthesis of Fe-Pd [18], Ni-Ti [19], and Cu-Al-Ni [20] by sputter depositing and subsequent quenching have been reported in the literature. In thin film studies, epitaxy may be induced via growth on a single-crystal substrate, which dictates the crystal growth direction of the film. As a refractory, electrically insulating, and transparent substrate, MgO offers a flat interface for epitaxial growth. It shows a convenient lattice that matches many metals with face-centered cubic symmetry [21].

For thin film synthesis using in situ heating, epitaxial growth can be provided by techniques such as laser ablation [22], molecular beam epitaxy [23,24], and electron beam evaporation [25]. Since preferential orientation is favored, the enhancement of shape memory properties can be achieved. Among the sputtered shape memory alloys, Ni-Ti [26] and Ni_2MnGa [27,28] are the systems for which in-depth research on epitaxial growth is being carried out.

Cu-Al-Ni SMAs are known for their good thermal and electrical conductivity, broad interval of transformation temperatures (between 70 and 470 K), good thermal stability of martensitic transformation, and large recoverable strains [29–31]. They typically have Ni and Al contents between 2–5 wt.% and 13–15 wt.%, respectively [32,33]. Cu-Al-Ni SMAs have some advantages over the widely used Ni-Ti SMAs, such as a lower melting temperature, which facilitates composition control [34]. The fact that they have better corrosion resistance and a lower cost compared to Ni-Ti, which is prone to oxidation, makes Cu-Al-Ni components favorable choices [35] for certain applications. Furthermore, it has been shown that achieving further enhancement in the microstructure and mechanical properties of Cu-Al-Ni SMAs is possible via the minor addition of cobalt to its composition [34]. The structural and mechanical properties of the Cu-Al-Ni system have been studied both for bulk alloys, which are produced by methods such as rapid solidification, casting [36], and powder metallurgy [37], and thin films, which are produced by methods including electron beam evaporation [38], thermal evaporation [39], and sputtering [40,41].

Here, the dependence of the crystallographic phase structure on the chemical composition of the Cu-Al-Ni shape memory system is reported for the first time for sputtered thin films. Different compositions were synthesized by adjusting the Al and Ni content. Additionally, the crystallographic differences due to the undertaken synthetic approach were investigated. Two methods were implemented to produce the thin films. Firstly, free-standing films with varying compositions were prepared by sputtering multilayers of Cu-Ni and Al. The as-grown films were conventionally annealed at 800 °C and quenched in iced water, as would be done in a top-down approach, in order to obtain a set of samples with different chemical compositions: Cu-14Al-4Ni (wt.%), Cu-13Al-5Ni (wt.%) and Cu-12Al-7Ni (wt.%). Secondly, Cu-12Al-7Ni (wt.%) thin films were grown on MgO(001) substrates

held at 700 °C, taking advantage of the epitaxial relationship between MgO(001) and austenitic β-Cu-Al-Ni as a bottom-up approach. Unlike most of the previous studies for sputtered Cu-Al-Ni samples, where a Cu-Al-Ni target was used for synthesis [16,27,34], in this work all depositions used individual Cu, Al, and Ni targets (i.e., co-sputtering). Structural characterization studies were carried out to investigate the crystallographic properties of the films. The martensitic phase transformation behavior of the samples was also investigated.

2. Materials and Methods

Cu, Al and Ni targets of 99.95% purity were used to grow all samples. In order to produce free-standing Cu-Al-Ni films, Si substrates were covered with resin by spin coating before sputtering. The deposition of multilayers was carried out by DC sputtering from Cu and Al targets and RF sputtering from a Ni target. Seven multilayers consisting of three Al films deposited between Cu-Ni films were prepared (Figure 1a). After the deposition, the samples were rinsed first in acetone and later in ethanol to dissolve the resin and to separate the film from the substrate. In order to promote diffusion to obtain a homogeneous composition, the films, wrapped in Ta foils, were subjected to annealing at 800 °C for 60 min in a sealed quartz tube and subsequently quenched in iced water.
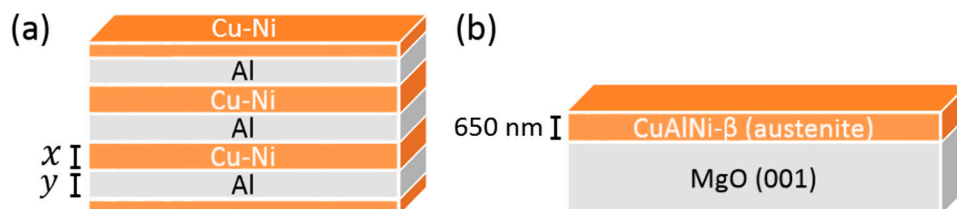

Figure 1. Sketch of the (**a**) prepared Cu-Ni/Al multilayers before quenching (for x and y values refer to Table 1) and (**b**) Cu-Al-Ni film on (001) oriented MgO.

Table 1. Thickness values of the sputtered multilayers before quenching. The top and bottom Cu–Ni layers have half the thickness of the layers in between.

Composition	Layer Thickness (nm)		Total Thin Film Thickness (nm)
	Cu-Ni (x)	Al (y)	Cu-Al-Ni
Cu-14Al-4Ni (wt.%)	230	58	864
Cu-13Al-5Ni (wt.%)	242	63	915
Cu-12Al-7Ni (wt.%)	347	70	1250

The top and bottom Cu-Ni layers had half the thickness of the Cu-Ni layers in between (Figure 1a). The details of the thickness values for each composition are given in Table 1, while sputtering conditions are listed in Table 2.

Table 2. The power (W) and time (min) conditions applied for the sputtering of samples Cu–14Al–4Ni (wt.%), Cu–13Al–5Ni (wt.%), and Cu–12Al–7Ni (wt.%).

Composition	Cu-Ni			Al	
	P (W)		t (min)	P (W)	t (min)
	Cu	Ni			
Cu-14Al-4Ni (wt.%)	200	60	10	200	14
Cu-13Al-5Ni (wt.%)	200	75	9	200	15.5
Cu-12Al-7Ni (wt.%)	200	85	10	200	17

The co-sputtered 650 nm thick Cu-12Al-7Ni (wt.%) thin film was deposited onto a 700 °C heated MgO(001) substrate (Figure 1b) from individual Cu, Al, and Ni targets using powers of 22, 30, and 5 W,

respectively. The deposition pressure was set to 0.65 Ar, and the deposition rate was approximately 4.3 nm/min.

Compositional analyses were performed with a field emission scanning electron microscope (FE-SEM, Zeiss, Oberkochen, Germany) equipped with an energy dispersive X-ray spectroscopy (EDX) detector operated at 15 kV. To confirm the homogeneity of the film along its thickness, EDX analysis was also carried out on the film cross-section. Structural characterization was carried out by X-ray diffraction (XRD, PANalytical, Royston, UK) (θ/2θ diffraction with Cu Kα radiation) and transmission electron microscopy (TEM, JEOL 2011 200 KV, Peabody, MA, USA). For TEM observations, the free-standing films were prepared with a GATAN polishing ion device (Pleasanton, CA, USA) while the Cu-12Al-7Ni (wt.%) film grown on MgO was scratched from the substrate and milled with an agate mortar. A Brucker D8 theta/theta four circle diffractometer (Billerica, MA, USA): Ω, 2θ, X, Φ, graded mirror (GM; to give a nearly parallel beam) equipped with a scintillation counter detector was used to study the epitaxial films grown on MgO. Coating thickness measurements were made using the 3D optical surface metrology system, Leica DCM 3D (Leica Microsystems Inc., Buffalo Grove, IL, USA). In order to investigate martensitic transformation behavior, electrical resistance measurements were performed with a 2 K/min heating rate.

3. Results and Discussion

The XRD patterns of films synthesized by both routes are shown in Figure 2a. Among the free-standing thin films produced by multilayer deposition, Cu-14Al-4Ni (wt.%) (Figure 2a) showed a mixture of β′ martensite and pure Cu. β′ martensite had a monoclinic structure (space group Cmcm), whereas Cu had a cubic Fm-3m lattice. As the content of Ni increased at the expense of Al, traces of β austenite (space group Fm-3m) along with β′ martensite were detected for Cu-13Al-5Ni (wt.%) (Figure 2b), and only β austenite was seen in the XRD pattern of Cu-12Al-7Ni (wt.%) (Figure 2c). In turn, the XRD pattern of the thin film co-sputtered at a high temperature on MgO mainly consisted of textured β austenite, but the Cu_9Al_4 phase (space group P-43m) was also present (Figure 2d). Previous studies on Cu-Al-Ni bulk shape memory alloys have reported that a slight change in composition results in a shift in the transformation temperatures [33,41,42]. The studies carried out by Recarté et al. revealed that, for a fixed aluminum content of 13.2 wt.%, a decrease in nickel from 5 wt.% to 3.5 wt.% raised the austenite finish temperature from 10 to 80 °C [33]. Agafonov et al. showed that Al content variation from 14.98 wt.% to 13.03 wt.% caused a change in the room temperature phase from austenite to martensite for samples synthesized by casting and quenching in water [41]. Similar trends were observed by Suresh and Ramamurty [42] where, at room temperature, a Cu-13.4Al-4Ni (wt.%) alloy was in the martensite state, but a Cu-14.1Al-4Ni (wt.%) alloy was austenitic. In our work, we observed that a change in Ni content followed the same trend in the transformation temperatures as the results reported by Recarté et al. [33], but the opposite tendency than that reported in [33,41] was observed when the aluminum content was modified. This may be because in our case, we were modifying Ni and Al content simultaneously, and, consequently, our transformation temperatures were influenced by both Al and Ni.

The film grown on MgO(001) showed a Cu-12Al-7Ni (wt.%) composition. The epitaxial relationship MgO(001)[100]/Cu-Al-Ni(001)[110] was induced. The film grew with a 45° in-plane rotation on the cubic cell of the substrate. The lattice mismatch (*f*) between the cubic lattices is shown in Equation (1):

$$f = (\sqrt{2}a_{MgO} - a_{CuAlNi \ \beta}) / a_{CuAlNi \ \beta} \tag{1}$$

where $a_{MgO} = 4.212$ Å, $a_{CuAlNi \ \beta} = 5.836$ Å.

The lattice mismatch between the film and the substrate was *f* = 2%, which was small enough to favor epitaxy. The epitaxial film, grown at 700 °C, exhibited preferential (100) out-of-plane orientation. This showed up as strong (200) and (400) peaks in the XRD pattern (Figure 2d). Peaks belonging to the Cu_9Al_4 phase (i.e., (200), (421), (332), and (550) planes) were also present. The formation of α-Cu and

Cu_9Al_4 phases is typically observed in Cu-Al-Ni systems [43,44]. The β phase in the Cu-Al-Ni system undergoes a eutectoid decomposition at ~840 K into α (Cu) and γ2 (Cu_9Al_4), then, the stable phases at room temperature are Cu and Cu_9Al_4. However, if the alloy is quenched at a sufficiently high cooling rate from the β phase region to ambient temperature, the β phase may be retained or it may transform martensitically. However, if the cooling rate is not high enough, traces of Cu or Cu_9Al_4 may be present in the alloy.
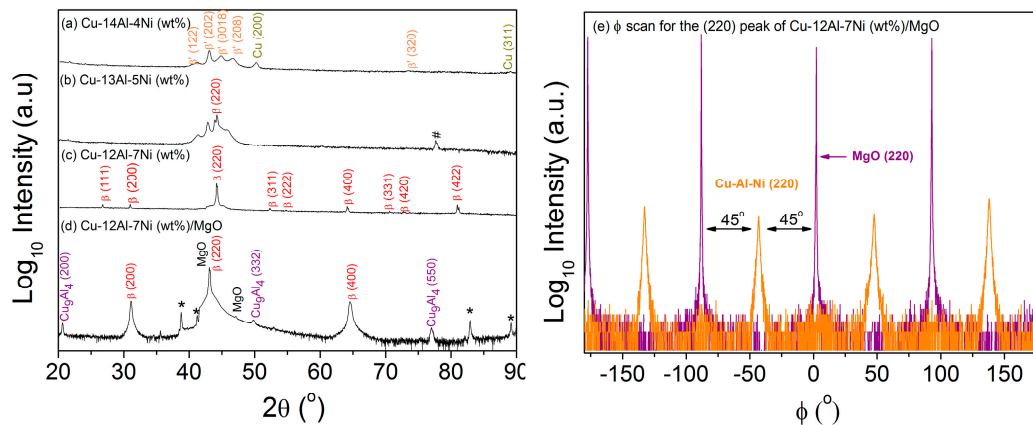
Figure 2. XRD patterns of the sputtered Cu–Al–Ni thin films: (**a**) θ/2θ scan for Cu–14Al–4Ni (wt.%); (**b**) θ/2θ scan for Cu–13Al–5Ni (wt.%); (**c**) θ/2θ Cu–12Al–7Ni (wt.%) films obtained by multilayer sputter deposition and subsequent heat treatment; (**d**) θ/2θ scan for Cu–12Al–7Ni (wt.%) film prepared on MgO substrate at 700 °C; and (**e**) φ scan for the (220) peak of the β–Cu–Al–Ni film deposited at 700 °C on MgO(001). # peak is unidentified. * peaks originate from the sample holder.

The phi scan carried out for the (220) peak of this film confirmed that the film lattice was rotated 45° in-plane, relative to the substrate (Figure 2e).

For the free-standing thin films produced by multilayer deposition, further evidence that the compositional change from Cu-14Al-4Ni (wt.%) to Cu-12Al-7Ni (wt.%) resulted in a shift from martensite to austenite was observed by TEM (Figure 3). Figure 3a,c shows TEM images of Cu-14Al-4Ni (wt.%) and Cu-12Al-7Ni (wt.%) thin films, respectively. Typical martensitic plates were present in Cu-14Al-4Ni, while a regular polycrystalline structure was observed in the Cu-12Al-7Ni (wt.%) alloy. The Selected Area Electron Diffraction (SAED) pattern from Cu-14Al-4Ni (wt.%) thin film (Figure 3b) consisted of diffraction spots that belong to β′ martensite corresponding to the (040), (202), (0018), (202), and (122) planes and to Face-Centered Cubic (FCC) Cu (i.e., (220), (311), (311), and (033) planes). Conversely, the SAED pattern of the Cu-12Al-7Ni (wt.%) thin film (Figure 3d) consisted of diffraction spots characteristic of the austenitic phase (β) corresponding to (111), (511), (711), (622), (422), and (533) planes. In Figure 4a, a high resolution TEM image of the epitaxial Cu-12Al-7Ni (wt.%) thin film grown on MgO is shown. From the fast-Fourier transform (FFT) pattern of the selected zone shown in Figure 4a, an interplanar distance value of 2.07 Å (which belongs to β austenite (220)), as well as a distance of 2.93 Å (which belongs to β austenite (200)), was identified (Figure 4b).

In order to identify the transformation temperatures, electrical resistance measurements were carried out as a function of temperature for both the quenched multilayered sample with the composition Cu-12Al-7Ni (wt.%) and the sample with the same composition grown on MgO. Martensitic transformation was not observed in the quenched multilayered Cu-12Al-7Ni (wt.%) (Figure 5a), whereas a trend that might be indicative of transformation hysteresis was found for the epitaxially grown Cu-12Al-7Ni (wt.%) sample (Figure 5b). The reason behind the fact that a transformation was observed in the epitaxially grown (200) textured austenite thin film whereas no change was seen in the randomly oriented polycrystalline one could be related to size effects. Size effects, such as the volume of the material or structural components including precipitate particles and grains in polycrystals, have a huge influence on the martensitic phase transformation [37]. Decreasing grain size

and decreasing twin separation cause an increase in strain energy and twin interfacial energy which, in turn, increases the energy barrier [38]. For instance, Shi et al. [39] showed that for submicrometric NiTi particles (below 100 nm), the martensitic transformation was fully suppressed. Similarly, in our work, no transformation was observed in the randomly oriented polycrystalline austenitic Cu-12Al-7Ni (wt.%) film with a crystallite size of 95 nm according to Scherrer's formula.
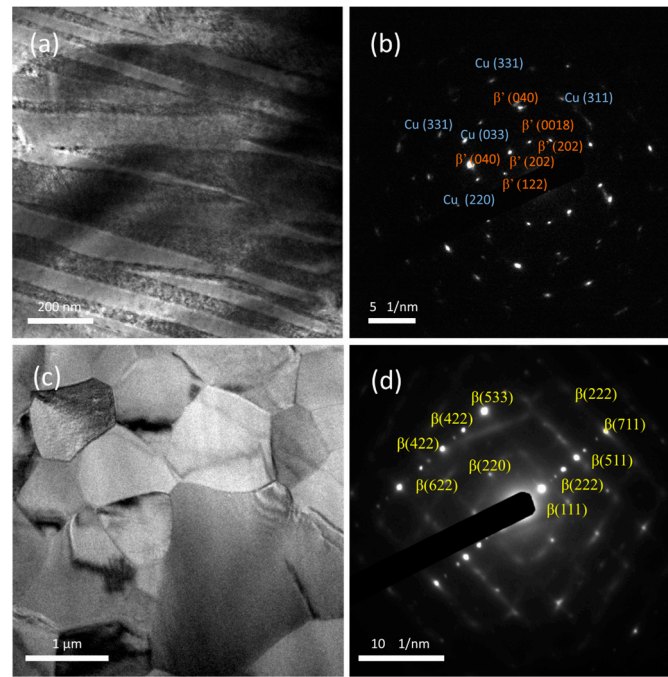

Figure 3. (**a**) Transmission electron microscopy (TEM) image of Cu–14Al–4Ni (wt.%) thin film produced from multilayer deposition followed by annealing; (**b**) SAED pattern of (**a,c**) TEM image of Cu–12Al–7Ni (wt.%) thin film; (**d**) SAED pattern of (**c**).
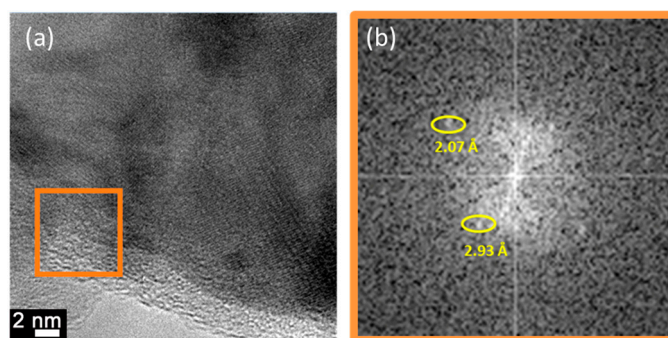
Figure 4. (**a**) HRTEM image of Cu–12Al–7Ni (wt.%) thin film grown on MgO; (**b**) FFT of the selected zone (orange square) in (**a**).

Additionally, previous studies demonstrate that decreasing film thickness is also a reason for the suppression of martensitic phase transformation [45–48]. Wan and Komvopoulos [48] showed that for sputtered NiTi films with a thickness of less than 100 nm, no martensitic transformation was observed. In the case of sputtered polycrystalline Cu-Al-Ni films, transformation temperatures for films with 2 μm thickness were reported by Moran and his co-workers [31]. To the best of our knowledge, these are the sputtered Cu-Al-Ni SMA films with the lowest thickness values reported in the literature. Torres et al. [20] also observed martensitic transformation for 5 μm thick films. In contrast, no transformation was observed in the polycrystalline 1.25 μm Cu-12Al-7Ni (wt.%) sample prepared in this work by post-treatment of the multilayers. It has been indicated by Chen and Schuh [49]

that as *d*(grain size)/*D*(sample thickness) decreases, the energy barrier for transformation increases. The interfacial energies depend on grain boundaries formed between martensite plates, the interfaces between austenite and martensite plates, and the twin interfaces within martensite plates [48].
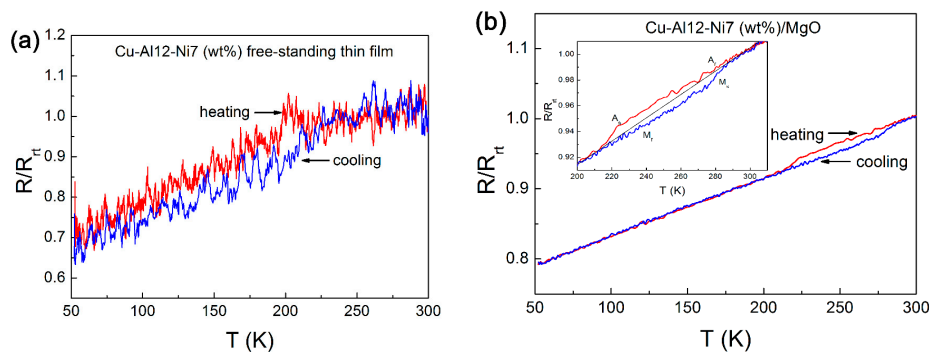

Figure 5. Resistance vs. temperature measurement of Cu–12Al–7Ni (wt.%) films prepared by (**a**) heat treatment after sputtering and (**b**) in situ heating during growth.

The absence of phase transformation in films formed at low deposition temperatures could be attributed to the small grain sizes causing a higher number of grain boundary interfaces and associated excess free volume, and/or the thinner nature of the samples, as noted by Wan and Komvopoulos [48].

4. Conclusions

In this work, structural characterization studies were carried out to investigate the crystallographic properties of Cu-Al-Ni films and their transformation temperatures.

The main conclusions from this work are as follows:

- The microstructure of Cu-Al-Ni sputtered films is found to depend both on the alloy composition as well as the experimental procedure used to grow the films.
- A transition from martensite to austenite was observed as the Ni content increased and the Al content decreased in samples prepared by multilayer sputtering followed by quenching.
- Preferential growth along the (100) direction was observed in β-austenite Cu-12Al-7Ni (wt.%) grown on MgO at 700 °C due to the epitaxial relationship MgO(001)[100]/Cu-Al-Ni(001)[110].
- Resistance change with respect to temperature, suggesting martensitic transformation hysteresis, was observed in the preferentially oriented austenitic Cu-12Al-7Ni (wt.%) film, whereas martensitic transformation was completely suppressed in the polycrystalline austenitic sample produced by multilayer sputtering with the same composition.

Conflicts of Interest: The authors declare no conflict of interest.

References

1. Otsuka, K.; Wayman, C.M. *Shape Memory Materials*; Cambridge University Press: Cambridge, UK, 1999.
2. Ma, J.; Karaman, I. Expanding the repertoire of shape memory alloys. *Science* **2010**, *327*, 1468–1469. [CrossRef]
3. Cingolani, E.; Ahlers, M.; Van Humbeeck, J. Stabilization and two-way shape memory effect in Cu-Al-Ni single crystals. *Met. Mater. Trans. A* **1999**, *30*, 493–499. [CrossRef]
4. Ishibashi, M.; Tabata, N.; Suetake, T.; Omori, T.; Sutou, Y.; Kainuma, R.; Yamauchi, K.; Ishida, K. A simple method to treat an ingrowing toenail with a shape-memory alloy device. *J. Dermatol.* **2008**, *19*, 291–292. [CrossRef] [PubMed]
5. Seelecke, S.; Muller, I. Shape memory alloy actuators in smart structures: Modeling and simulation. *Appl. Mech. Rev.* **2004**, *57*, 23–46. [CrossRef]
6. Jani, J.M.; Leary, M.; Subic, A.; Gibson, M.A. A review of shape memory alloy research, applications and opportunities. *Mater. Des.* **2014**, *56*, 1078–1113. [CrossRef]
7. Montero-Ocampo, C.; Lopez, H.; Salinas Rodriguez, A. Effect of compressive straining on corrosion resistance of a shape memory Ni-Ti alloy in ringer's solution. *J. Biomed. Mater. Res.* **1993**, *32*, 583–591. [CrossRef]
8. Bogue, R. Shape-memory materials: A review of technology and applications. *Assem. Autom.* **2009**, *29*, 214–219. [CrossRef]
9. Dehghanghadikolaei, A.; Ibrahim, H.; Amerinatanzi, A.; Hashemi, M.; Moghaddam, N.S.; Elahinia, M. Improving corrosion resistance of additively manufactured nickel-titanium biomedical devices. *J. Mater. Sci.* **2019**, *54*, 7333–7355. [CrossRef]
10. Eggeler, G.; Hornbogen, E.; Yawny, A.; Heckmann, A.; Wagner, M. Structural and functional fatigue of NiTi fhape memory alloys. *Mater. Sci. Eng. A* **2004**, *378*, 24–33. [CrossRef]
11. Ibrahim, H.; Jahadakbar, A.; Dehghan, A.; Moghaddam, N.S.; Amerinatanzi, A.; Elahinia, M. In vitro corrosion assessment of additively manufactured porous NiTi structures for bone fixation applications. *Metals* **2018**, *8*, 164. [CrossRef]
12. Perkins, J.; Sponholz, R.O. Stress-induced martensitic transformation cycling and two-way shape memory training in Cu-Zn-Al alloys. *Met. Mater. Trans. B* **1984**, *15*, 313–321. [CrossRef]
13. Ivanić, I.; Kožuh, S.; Grgurić, T.H.; Kosec, B.; Gojić, M. The influence of heat treatment on microstructure and phase transformation temperatures of Cu-Al-Ni shape memory alloys. *Kem. Ind.* **2019**, *68*, 111–118. [CrossRef]
14. Recarte, V.; Pérez-Landazábal, J.I.; Ibarra, A.; Nó, M.L.; San Juan, J. High temperature β phase decomposition process in a Cu-Al-Ni shape memory alloy. *Mater. Sci. Eng. A* **2004**, *378*, 238–242. [CrossRef]
15. Alaneme, K.K.; Okotete, E.A. Reconciling viability and cost-effective shape memory alloy options–A review of copper and iron based shape memory metallic systems. *Eng. Sci. Technol. Int. J.* **2016**, *19*, 1582–1592. [CrossRef]
16. Pan, Q.; Cho, C. The investigation of a shape memory alloy micro-damper for MEMS applications. *Sensors* **2007**, *7*, 1887–1900. [CrossRef]
17. Olson, G.B.; Cohen, M. A general mechanism of martensitic nucleation: Part I. General concepts and the FCC → HCP transformation. *Metall. Mater. Trans. A* **1976**, *7*, 1897–1904.
18. Sugimura, Y.; Cohen-Karni, I.; McCluskey, P.; Vlassak, J. Stress evolution in sputter-deposited Fe–Pd shape-memory thin films. *J. Mater. Res.* **2005**, *20*, 2279–2287. [CrossRef]
19. Chu, J.P.; Lai, Y.W.; Lin, T.N.; Wang, S.F. Deposition and characterization of TiNi-base thin films by sputtering. *Mater. Sci. Eng. A* **2000**, *277*, 11–17. [CrossRef]
20. Torres, C.E.; Condo, A.; Haberkorn, N.; Zelaya, E.; Schryvers, D.; Guimpel, J.; Lovey, F. Structures in textured Cu–Al–Ni shape memory thin films grown by sputtering. *Mater. Charact.* **2014**, *96*, 256–262. [CrossRef]
21. Tolstova, Y.; Omelchenko, S.T.; Shing, A.M.; Atwater, H.A. Heteroepitaxial growth of Pt and Au thin films on MgO single crystals by bias-assisted sputtering. *Sci. Rep.* **2016**, *6*, 23232. [CrossRef]
22. Gu, H.; You, L.; Leung, K.; Chung, C.; Chan, K.; Lai, J. Growth of TiNiHf shape memory alloy thin films by laser ablation of composite targets. *Appl. Surf. Sci.* **1998**, *127*, 579–583. [CrossRef]
23. Dong, J.W.; Chen, L.C.; Palmstro/m, C.J.; James, R.D.; McKernan, S. Molecular beam epitaxy growth of ferromagnetic single crystal (001) Ni_2MnGa on (001) GaAs. *Appl. Phys. Lett.* **1999**, *75*, 1443–1445. [CrossRef]

24. Shih, T.C.; Xie, J.Q.; Dong, J.W.; Dong, X.Y.; Srivastava, S.; Adelmann, C.; McKernan, S.; James, R.D.; Palmstrøm, C.J. Epitaxial growth and characterization of single crystal ferromagnetic shape memory Co$_2$NiGa films. *Ferroelectrics* **2006**, *342*, 35–42. [CrossRef]

25. Kühnemund, L.; Edler, T.; Kock, I.; Seibt, M.; Mayr, S.G. Epitaxial growth and stress relaxation of vapor-deposited Fe-Pd magnetic shape memory films electron beam evaporation. *New J. Phys.* **2009**, *11*, 113054. [CrossRef]

26. Gisser, K.R.C.; Busch, J.D.; Johnson, A.D.; Ellis, A.B. Oriented nickel-titanium shape memory alloy films prepared by annealing during deposition. *Appl. Phys. Lett.* **1992**, *61*, 1632–1634. [CrossRef]

27. Jenkins, C.A.; Ramesh, R.; Huth, M.; Eichhorn, T.; Pörsch, P.; Elmers, H.J.; Jakob, G. Growth and magnetic control of twinning structure in thin films of Heusler shape memory compound Ni$_2$MnGa. *Appl. Phys. Lett.* **2008**, *93*, 234101. [CrossRef]

28. Niemann, R.; Backen, A.; Kauffmann-Weiss, S.; Behler, C.; Rößler, U.; Seiner, H.; Heczko, O.; Nielsch, K.; Schultz, L.; Fähler, S. Nucleation and growth of hierarchical martensite in epitaxial shape memory films. *Acta Mater.* **2017**, *132*, 327–334. [CrossRef]

29. Goryczka, T. Effect of wheel velocity on texture formation and shape memory in Cu-Al-Ni melt-spun ribbons. *Arch. Metall. Mater.* **2009**, *54*, 755–763.

30. Delaey, L. Diffusionless transformations. In *Phase Tranformation in Materials*; Kostorz, G., Ed.; Wiley-VCH: Weinheim, Germany, 2001.

31. Morán, M.; Condó, A.; Soldera, F.; Sirena, M.; Haberkorn, N. Martensitic transformation in freestanding and supported Cu–Al–Ni thin films obtained at low deposition temperatures. *Mater. Lett.* **2016**, *184*, 177–180. [CrossRef]

32. Niedbalski, S.; Durán, A.; Walczak, M.; Ramos-Grez, J.A. Laser-assisted synthesis of Cu-Al-Ni shape memory alloys: Effect of inert gas pressure and Ni content. *Materials* **2019**, *12*, 794. [CrossRef]

33. Recarte, V.; Pérez-Sáez, R.B.; Juan, J.S.; Bocanegra, E.H.; Nó, M.L. Influence of Al and Ni concentration on the Martensitic transformation in Cu-Al-Ni shape-memory alloys. *Met. Mater. Trans. A* **2002**, *33*, 2581–2591. [CrossRef]

34. Braga, F.D.O.; Matlakhov, A.N.; Matlakhova, L.A.; Monteiro, S.N.; De Araújo, C.J. Martensitic transformation under compression of a plasma processed polycrystalline shape memory CuAlNi Alloy. *Mater. Res.* **2017**, *20*, 1579–1592. [CrossRef]

35. Haidar, M.A.; Saud, S.N.; Hamzah, E. Microstructure, mechanical properties, and shape memory effect of annealed Cu-Al-Ni-*x*Co shape memory alloys. *Metallogr. Microstruct. Anal.* **2018**, *7*, 57–64. [CrossRef]

36. Saud, S.N.; Bakar, T.A.A.; Hamzah, E.; Ibrahim, M.K.; Bahador, A. Effect of quarterly element addition of cobalt on phase transformation Cu-Al-Ni shape memory alloys. *Metall. Mater. Trans. A* **2015**, *46*, 3528–3542. [CrossRef]

37. Sharma, M.; Vajpai, S.K.; Dube, R.K. Processing and characterization of Cu-Al-Ni shape memory alloy strips prepared via a novel powder metallurgy route. *Metall. Mater. Trans. A* **2010**, *41*, 2905–2913. [CrossRef]

38. Gómez-Cortés, J.; Juan, J.S.; Lopez, G.A.; Nó, M. Synthesis and characterization of Cu–Al–Ni shape memory alloy multilayer thin films. *Thin Solid Films* **2013**, *544*, 588–592. [CrossRef]

39. Canbay, C.A.; Tekatas, A.; Ozkul, I. Fabrication of Cu-Al-Ni shape memory thin film by thermal evaporation. *Turk. J. Eng.* **2017**, *1*, 27–32.

40. Minemura, T.; Andoh, H.; Kita, Y.; Ikuta, I. Shape memory effect and microstructures of sputter-deposited Cu-Al-Ni films. *J. Mater. Sci. Lett.* **1985**, *4*, 793–796. [CrossRef]

41. Agafonov, V.; Naudot, P.; Dubertret, A.; Dubois, B. Influence of the aluminium content on the appearance and stability of martensites in the Cu Al Ni system. *Scr. Met.* **1988**, *22*, 489–494. [CrossRef]

42. Suresh, N.; Ramamurty, U. Aging response and its effect on the functional properties of Cu–Al–Ni shape memory alloys. *J. Alloy. Compd.* **2008**, *449*, 113–118. [CrossRef]

43. Sharma, M.; Vajpai, S.K.; Dube, R.K.; Vajpai, S. Synthesis and properties of Cu–Al–Ni shape memory alloy strips prepared via hot densification rolling of powder preforms. *Power Metall.* **2011**, *54*, 620–627. [CrossRef]

44. Araujo, A.P.M.; Simões, J.B.; Araújo, C.J. Analysis of compositional modification of commercial aluminum bronzes to obtain functional shape memory properties. *Mater. Res.* **2017**, *20*, 331–341. [CrossRef]

45. Malygin, G.A. Nanoscopic size effects on martensitic transformations in shape memory alloys. *Phys. Solid State* **2008**, *50*, 1538–1543. [CrossRef]

46. Waitz, T.; Karnthaler, H. Martensitic transformation of NiTi nanocrystals embedded in an amorphous matrix. *Acta Mater.* **2004**, *52*, 5461–5469. [CrossRef]

47. Shi, X.; Cui, L.; Jiang, D.; Yu, C.; Guo, F.; Yu, M.; Ren, Y.; Liu, Y. Grain size effect on the R-phase transformation of nanocrystalline NiTi shape memory alloys. *J. Mater. Sci.* **2014**, *49*, 4643–4647. [CrossRef]

48. Wan, D.; Komvopoulos, K. Thickness effect on thermally induced phase transformations in sputtered titanium-nickel shape-memory films. *J. Mater. Res.* **2005**, *20*, 1606–1612. [CrossRef]

49. Chen, Y.; Schuh, C.A. Size effects in shape memory alloy microwires. *Acta Mater.* **2011**, *59*, 537–553. [CrossRef]